

Photophysics of Glycosylated Ring-Fused Chlorin Complexes and Their Photosensitizing Effects on Cancer Cells

Ingvild U. Hageberg⁺,^[a] Katrianne Arja⁺,^[b] Benedikte E. Vindstad,^[a] Johannes K. Bergvoll,^[a] Odrun A. Gederaas,^[c] Thor-Bernt Melø,^[a] K. Peter R. Nilsson,^[b] and Mikael Lindgren^{*[a]}

The future of photodynamic therapy (PDT) as a promising cancer treatment relies on the development of new selective and effective photosensitizers (PS) with improved photophysical and biochemical qualities. Herein, we present the synthetic procedure, photophysical properties and photosensitizing effects of novel glycosylated 4,5,6,7-tetrahydropyrazolo[1,5-a]pyridine fused chlorin agents featuring either glucose, galactose, or N-acetyl glucosamine. It is shown that both the proto- and Zn²⁺-ion forms of the ring-stabilized glyochlorins exhibit the required photophysical properties in terms of triplet excited states and singlet oxygen generation, the latter more than 50% in organic solvents such as CHCl₃. Employing the rat

AY-27 and human T24 cancer cell models, it was found that these are superior to the corresponding unglycosylated chlorin in biological activity, and moreover, the proto form is 2–3 times superior to the Zn-stabilized variant. Provisional flow cytometry and cell localization studies of the proto-form indicate both necrotic and apoptotic biological activity, and that the photosensitizer localizes in the mitochondria, cell membrane and lysosomes. However, the localization into the lysosomes is dominating and increases substantially with time. We anticipate the findings will aid in the development of photosensitizers for targeted cancer PDT.

Introduction

Photodynamic therapy (PDT) is a minimally invasive light-mediated cancer therapy involving a photosensitizer (PS) that is selectively localized in cancer cells, a light with a specific wavelength to excite the PS and molecular oxygen found in biological tissue.^[1,2] PDT owes its promising future prospects to the fact that it can be made dually selective towards malignant tissue by designing photoactive drugs that are selectively accumulating in cancer cells and by choosing the right spatio-temporal parameters for activating the drug by light irradiation.^[3] After absorbing a photon, the PS is converted to

its triplet excited state via the process of intersystem crossing (ISC) where it interacts with molecular oxygen, producing highly oxidizing singlet oxygen and other reactive oxygen species (ROS).^[4] In cancer cells, ROS cause oxidative damage in amino acids and DNA bases as well as the sugar backbone of the DNA, to the degree that the cells are not able to repair and replicate, leading to cell death.^[5]

Tetrapyrrolic macrocycles, also known as porphyrinoids, have over the years shown to possess a wide range of attractive properties based on their interesting photophysical nature of high absorption and conversion of visible light to chemical and electrical energy.^[6] These naturally occurring compounds are now the most well-studied structures as photosensitizers for PDT to treat an array of medical conditions, including bacterial, fungal, and virus infections and skin conditions such as acne and psoriasis, but most importantly oncological disorders.^[7,8,9]

Among porphyrin-based photosensitizers Photofrin® was the first one to receive its FDA regulatory approval for clinical use in 1995,^[10] have gone through three generations of development striving to meet the criteria for successful PDT. These criteria include a well-defined chemical structure with advantageous biodistribution, and pharmacokinetics including high cellular uptake and cancer cell selectivity. A combination of minimal dark-toxicity and high phototoxicity, together with absorption within the “therapeutic window” of 600–800 nm for effective light penetration in biological tissue are important requirements.^[11] There has been intensive research on design and evaluation of photosensitizers considering the different aspects of the above-mentioned criteria.^[3] In our previously published study we evaluated fluoroglycosylated porphyrins as potential agents for combined therapeutics and diagnostics.^[12]

[a] I. U. Hageberg,⁺ B. E. Vindstad, J. K. Bergvoll, Prof. T.-B. Melø, Prof. M. Lindgren
Department of Physics
Norwegian University of Science and Technology
7491 Trondheim (Norway)
E-mail: mikael.lindgren@ntnu.no

[b] Dr. K. Arja,⁺ Prof. K. P. R. Nilsson
Division of Chemistry
Department of Physics, Chemistry and Biology
Linköping University
581 83 Linköping (Sweden)

[c] Prof. O. A. Gederaas
Department of Natural Science
University of Agder, 4630 Kristiansand (Norway)

[⁺] These authors contributed equally to this work.

Supporting information for this article is available on the WWW under <https://doi.org/10.1002/cptc.202300028>

© 2023 The Authors. ChemPhotoChem published by Wiley-VCH GmbH. This is an open access article under the terms of the Creative Commons Attribution Non-Commercial NoDerivs License, which permits use and distribution in any medium, provided the original work is properly cited, the use is non-commercial and no modifications or adaptations are made.

Here, a set of heterobifunctional glycoconjugated porphyrins was synthesized, featuring a common monosaccharide (glucose, galactose or N-acetyl glucosamine) at three sites and a 2-fluoro-2-deoxy glucose (FDG) moiety at the remaining site on the porphyrin periphery. The study successfully demonstrated improved cellular uptake into melanoma cells and enhanced cancer cell selectivity over fibroblasts of these carbohydrate-functionalized porphyrins, as compared to the corresponding unglycosylated porphyrin.^[12]

Besides the targeting aspect, we now broaden our focus towards improving the photophysical parameters of the PS core. Of common porphyrinoids, porphyrins are synthetically the easiest accessible and most stable, while their derivatives, e.g. chlorins and bacteriochlorins, are more complex and tedious to synthesize and have decreased chemical- and photostability.^[16] Porphyrins are therefore perfectly suitable for conceptual studies on the effect of targeting modalities. However, porphyrins show the least favorable absorption profiles of the porphyrinoids, having relatively low absorption within the therapeutic window. The absorption within this range increases when moving from porphyrins to chlorins (dihydroporphyrins),^[13] which early made this porphyrinoid variant subject for clinical studies, e.g., Foscan®,^[14] and Radachlorin®.^[15]

Different methodologies have been applied to produce chlorins, both using step-by-step synthesis from scratch^[17,18] or modifying a pre-existing porphyrin,^[19] and to avoid the back-oxidation of the chlorin core to porphyrin.^[18,20] A relatively convenient way to produce chlorins is cycloaddition of a precursor porphyrin in Diels-Alder or 1,3-dipolar cycloaddition reactions.^[19–21] Pereira et al. demonstrated a novel approach to stable chlorins employing $[8\pi + 2\pi]$ cycloaddition between easily accessible meso-arylporphyrins and *in situ* generated diazafulvenium methide.^[22–24] The reaction is regioselective leading to acceptable yields of 4,5,6,7-tetrahydropyrazolo[1,5-a]pyridine fused chlorins. These ring-fused chlorins owe their stability to the bond strain created along the fusion axes between the porphyrin core and the pyrazolo[1,5-a]pyridinium structure in case of the back-oxidation, thus keeping the chlorin in its saturation state. This type of 4,5,6,7-tetrahydropyrazolo[1,5-a]pyridine ring-fused chlorins have shown promising results as photosensitizers in *in vitro* PDT studies against human melanocytic melanoma and human amelanotic melanoma.^[25–27] There are also indications that some added hydrophilicity may improve the cellular uptake of these chlorins and therefore the total PDT effect.^[28,29] However, the literature does not reflect over any studies on cancer cell selectivity of this type of ring-fused chlorins nor have these macrocyclic systems been conjugated to any targeting modalities. Glycosylation is a well-known way to increase water-solubility and biocompatibility of therapeutically interesting molecules.^[30–34]

Herein, we present the synthesis and characterization of novel glycosylated chlorins and their potential as effective photosensitizers in PDT against malignant cells. In the current study we utilize the knowledge of our previous results from glycoporphyrins with enhanced cellular uptake and preferential

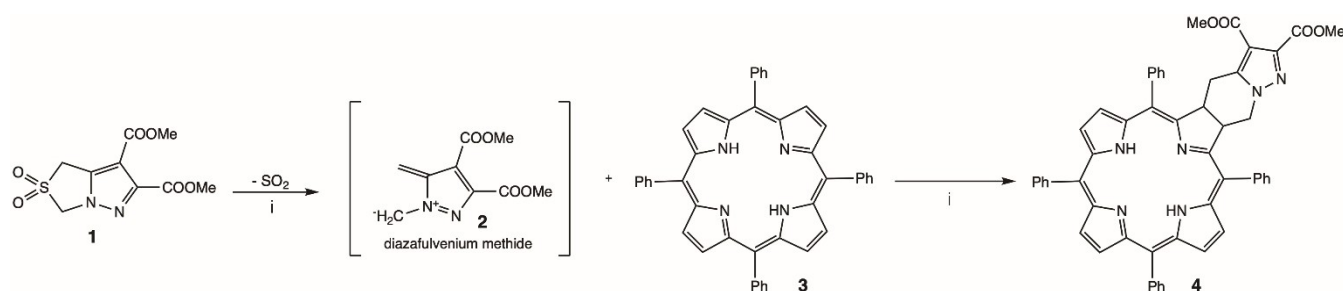
accumulation in cancer cells^[12] and apply it to the 4,5,6,7-tetrahydropyrazolo[1,5-a]pyridine fused chlorin scaffold with improved photophysical properties. In the applied synthetic strategy, we used an easily accessible starting material in form of 5,10,15,20-tetraphenyl porphyrin in $[8\pi + 2\pi]$ cycloaddition with *in situ* generated diazafulvenium methide to obtain the desired chlorin scaffold. We employed three different common monosugars (glucose, galactose and N-acetyl glucosamine) to equip the chlorin with water-soluble and malignant cell targeting modalities. The conjugation was done using the highly effective and selective copper(I) catalyzed azide alkyne Huisgen cycloaddition,^[34,35] producing a set of six glycosylated 4,5,6,7-tetrahydropyrazolo[1,5-a]pyridine fused chlorins featuring either two glucose, galactose or N-acetyl glucosamine moieties on the zinc-metallated macrocycle and on its unmetallated protoform. Photophysical evaluation of the glycochlorins demonstrated desired properties of a good photosensitizer with a considerable absorption maximum in the biologically relevant spectral range between 600–700 nm, the occurrence of a triplet state and the ability to generate singlet oxygen, similar to previous studies of related compounds.^[26,27,29,36] Moreover, fluorescence microscopy results from AY-27 and T24 cell models with the synthesized PSs show that glycoconjugation of the chlorin macrocycle contributes to high cellular uptake and substantial photodynamic effect.

Results and Discussion

Synthesis of Glycosylated 4,5,6,7-tetrahydropyrazolo[1,5-a]pyridine Fused Chlorins

The photosensitizable chlorin scaffold 4,5,6,7-tetrahydropyrazolo[1,5-a]pyridine fused chlorin was chosen for its robustness and simple preparation, as described above. Moreover, good stability in further functionalization reactions was a requirement, making the ring-fused chlorin a good candidate. Additionally, in the chlorin-forming pericyclic reaction used 8π -partner, S,S-dioxo-pyrazolothiazole, features two methyl ester groups providing the product with suitable sites for conjugation. Synthetically straightforwardly accessible 5,10,15,20-tetraphenyl porphyrin, TPP, was used as starting material owing to its complete symmetry avoiding formation of complex mixtures of regioisomers further in the synthetic work. To demonstrate feasible replacement of carbohydrate moieties on the chlorin chromophore, Cu(I)-catalyzed click-reaction was chosen for the conjugation chemistry.

The synthetic procedure of 4,5,6,7-tetrahydropyrazolo[1,5-a]pyridine fused chlorin 4 was adopted from Pereira et al.^[23,24] employing previously synthesized S,S-dioxo-pyrazolothiazole 1 in $[8\pi + 2\pi]$ cycloaddition between *in situ* formed diazafulvenium methide 2 as 1,7-dipole and TPP 3 as dipolarophile (Scheme 1). The yield of 26% is acceptable for this type of reaction, while a considerable part of the unreacted excess of TPP could be recovered. The synthesis of S,S-dioxo-pyrazolothiazole 1 followed previously published procedures starting



Scheme 1. General conditions and reagents for the preparation of compounds 2–4: i) 1,2,4-trichlorobenzene, 220 °C, 26 %.

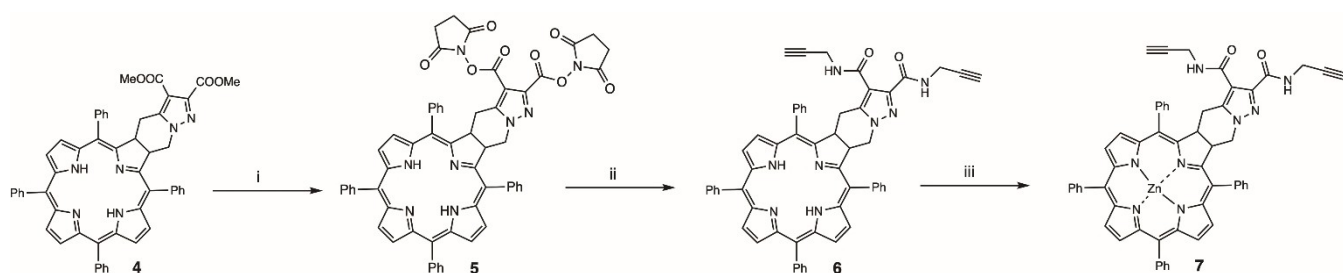
from (L)-thiazolidine-4-carboxylic acid and is fully described in Supporting Information (Scheme S1).^[37]

To facilitate the glycosylation of chlorin 4 through Cu(I)-catalyzed click reaction, the chlorin scaffold was functionalized with terminal alkyne groups (Scheme 2). The methyl esters on 4 were subsequently hydrolyzed with aqueous LiOH in refluxing dioxane. The overall hydrophobicity of the compound and possibly some contributing electronic effects, made the esters relatively resistant towards the demethylation, requiring harsher conditions and longer reaction times. However, HPLC-MS/UV monitoring of the reaction progression showed a distinct monohydrolyzed product, indicating the future possibility for functionalization one site at a time. The free carboxylic acids were turned into activated N-hydroxysuccinimide esters on 5 using EDC mediated coupling chemistry which was followed by alkylation with propargylamine, yielding bis-alkynylated chlorin 6 in 66% over three steps. In preparation for Cu(I)-catalyzed reaction, the chlorin equipped N-acetyl glucosamine 13 via Sharpless' modified Cu(I)-catalyzed Huisgen 1,3-cycloaddition was done according to previously worked-out microwave protocol^[35] and has been successfully employed by our group earlier (Scheme 3). 5 minutes microwave irradiation at 85 °C in sealed tubes with the presence of 0.25 mole equivalents of *in situ* generated Cu(I) gave glycochlorins 8, 9 and 10 in good yields. Deacetylation of the sugar moieties of 8, 9 and 10 using aqueous sodium hydroxide in THF at room temperature produced the set of glycosylated Zn-chlorins consisting of compound 14a, 15a and 16a. Proto-form glycochlorins 14b, 15b and 16b were produced by demetallation of the corresponding Zn-complexes by treatment with TFA:DCM, 1:4. Both the deacetylations and demetallations

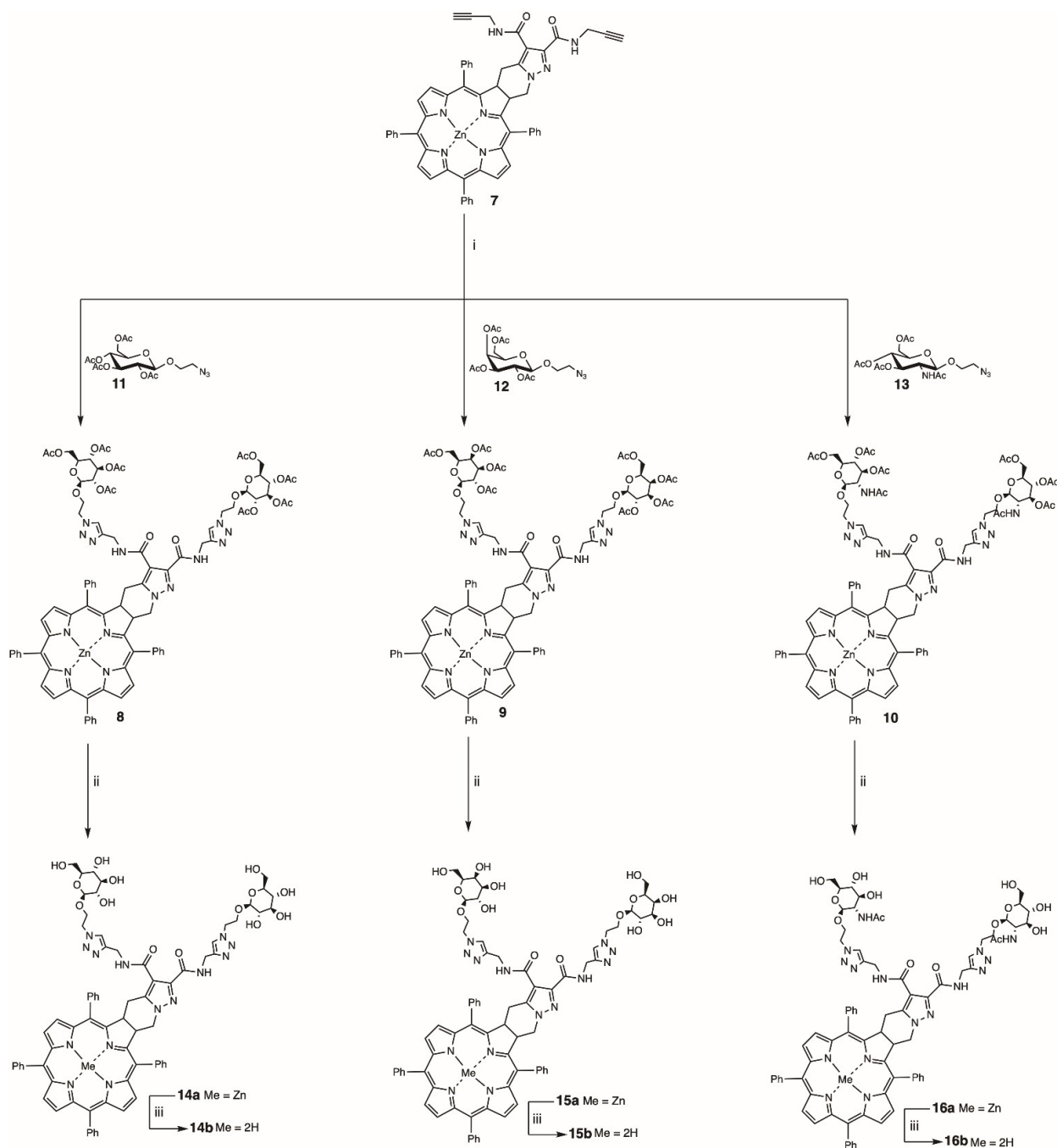
proceeded smoothly in nearly quantitative yields for all three glycochlorins. The identity and purity of all the intermediate compounds and final products were confirmed by HPLC-MS/UV-vis analysis as well as ¹H and ¹³C NMR. After glycoconjugation, the ¹H NMR analyses revealed the existence of conformational isomerism about the plane of the ring-fused chlorin as evident from the four different triazole proton peaks (Figure S1). We believe that these conformers result from the steric hindrance between the triazole-linkage to the carbohydrates and the adjacent phenyl groups, as there is no evidence for isomerism in chlorin scaffold 4 nor in alkynylated chlorin 6. Furthermore, in our previous work on glycoporphyrins, where the triazole-conjugation to the carbohydrates emerged from the phenylic para-positions of the porphyrin, no conformational isomerism was observed.^[12] Glycoconjugated chlorins 14–16 were further characterized for their basic photophysical properties including triplet excited states and singlet oxygen formation. Cell viability was examined using two different *in vitro* models (AY-27, T24) using both red and blue illumination. Finally, the proto-form was subjected to provisional flow cytometry and cell localization studies to elucidate the biological activity.

Absorption and emission properties

Absorption characteristics are important for the photo-initiation, and emission can be used to study the localization of the PS in cancer cell models. Representative absorption and emission spectra of compounds 6, 14a and 14b using EtOH as solvent are shown in Figure 1. The alkynylated chlorin 6 was



Scheme 2. General conditions and reagents for the preparation of compounds 5–7: i) 1. Aq. LiOH, dioxane, reflux; 2. Dowex, r.t.; 3. NHS, EDC, DMF, r.t.; ii) propargylamine, DIPEA, DMF, r.t., 66 % over three steps; iii) Zn(OAc)₂·2H₂O, MeOH, DCM, r.t. quant.



Scheme 3. General conditions and reagents for the preparation of compounds **14a,b**, **15a,b**, and **16a,b**: i) $\text{Cu}(\text{OAc})_2$, sodium L-(+)-ascorbate, $t\text{BuOH}$, THF, H_2O , MW 85°C , 52% (**11**), 70% (**12**), 56% (**13**); ii) aq. NaOH, THF, r.t. quant. (**14a**), quant. (**15a**), 96% (**16a**); iii) TFA, DCM, r.t. quant. (**14b**), quant. (**15b**), quant. (**16b**).

used as an unglycosylated reference to compare photophysical and photobiological alteration caused by the conjugated carbohydrate moieties.

Thus, the effect of glycosylation on **6** has very small spectral changes, manifested as the disappearance of the small band at 445 nm (compared to **14b**). Similar to previous results of ring-stabilized chlorins,^[24–27] the Soret band of the proto-form is at 420 nm and the Q-bands are at 520, 545, 600 and 650 nm, proving that the peripheral linkage to the carbohydrates does not affect the chromophore behavior. The Zn-form gives a

narrower Soret band, and a simpler substructure structure of the Q-band. The latter show a broad feature in the range 510–580 nm, and two distinct bands at around 590 and 625 nm. Similar spectra as in Figure 1 were obtained using solvents such as MeOH, EtOH and CHCl_3 . Using PBS there is a considerable broadening of all absorption bands. An important difference from our previously published glycoporphyrins relevant for PDT,^[12] is the significant increase of extinction coefficient in the longest-wavelength Q-band. The fluorescence emissions show distinct bands at 625 and 650 nm for the Zn-

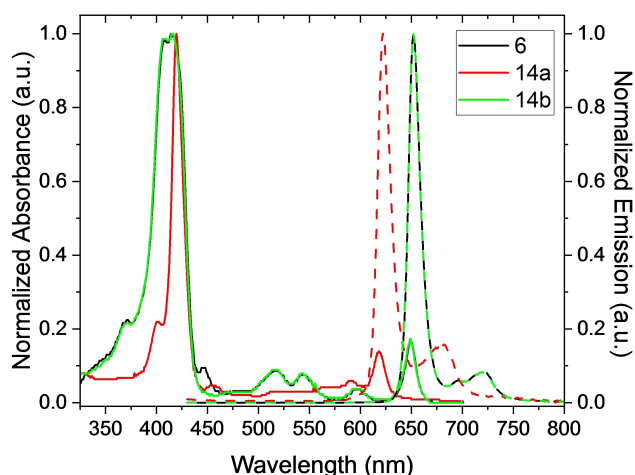


Figure 1. Absorption (solid lines) and emission (dashed lines) of **6**, **14a** and **14b**, in EtOH. For the emission spectra, the excitation wavelength was 422 nm. The spectra have been amplitude normalized for easy comparison of spectral band intensities and positions. Concentrations for photophysical studies were typically 0.5–2 μM .

and proto-forms, respectively. Solvent effects of absorption and emission spectra of **14a** and **14b** are shown in Figure S2 and spectra of all glycosylated forms in CHCl_3 are indeed very similar as shown in Figure S3.

The associated fluorescence decay times in the ns regime were measured using time-correlated single photon counting (TC SPC) and representative results for **15a** and **15b** in PBS and methanol are shown in Figure 2. The decay traces were drastically shortened when using PBS as solvent. The decay of **15a** falls upon the instrument response indicating a very short decay time < 100 ps, indicating a strong quenching. In PBS **15b** shows a distinct two-exponential decay with a dominating (78%) fast component < 80 ps and a longer component 8.5 ns, the latter contributing only 28% to the total amplitude (at $t =$

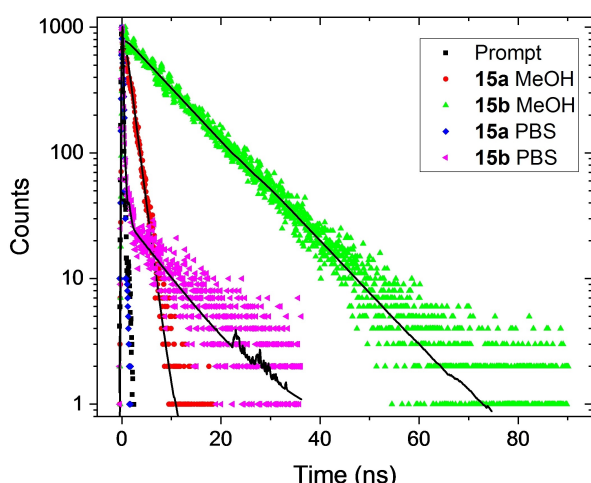


Figure 2. TCSPC traces of **15a** and **15b** in methanol and PBS. The excitation wavelength was 403 nm and the emission collected at 650 nm using a 32 nm slit to cover most of the emissions. The solid lines indicate fits to parameters summarized in Table 1. Concentrations for photophysical studies were typically 0.5–2 μM .

0). For non-aqueous solvents the decay-times are typically around 9–11 ns for the proto-form, but considerably shorter, ~ 1.5 ns, for the Zn-stabilized ring. The fitted parameters for different solvents for **15a** and **15b** are summarized in Table 1 (also Figure 2). Using an ideal solvent such as CHCl_3 , the decay traces of all glycosylated variants are essentially identical for the Zn- and proto-forms, respectively, see Figure S4.

The corresponding quantum efficiencies were found to be around 13% and 4.3% for the proto- and Zn-forms, respectively, using non-aqueous solvents (Table 2; Figure S5). As mentioned, different solvents had little effect on the emission band position except for a small redshift for PBS (Figures 2, S2, S3) but the associated quantum efficiency (QE) was drastically reduced using the latter, being only 2.2% and 0.1% for the proto- and Zn-forms, respectively. The latter in agreement with the strong quenching as judged from the shortened associated decay times (Figure 2, Table 1). Representative raw-data using two different QE reference standards are shown in Figure S5 and the calculated QEs using ethanol, chloroform and PBS for **14a** and **14b** are summarized in Table 2. The QE of the alkynated variant was slightly greater than the glycosylated proto variants, 19% (EtOH).

Conclusively, the basic absorption and emission properties of all glycosylated forms follows previous studies of similar ring-stabilized chlorins.^[24,25,36] As photo-sensitizers they can be excited blue light in the Soret band around 400–420 nm or with red light at the dominating peaks Q-bands at 625 nm (Zn) and 650 nm (proto), respectively. The investigation of cell localization will be feasible when localizing in non-aqueous cell compartments as quantum efficiency is drastically reduced in PBS.

Table 1. Fluorescence decay times of compound **15a** and **15b** in methanol (MeOH), ethanol (EtOH), butanol (BuOH), chloroform (CHCl_3) and PBS. The excitation was 403 nm and the emissions collected around 630–650 nm. 'W' denotes amplitude weight of the double-decay model.

Solvent	τ (ns) 15a	τ (ns) 15b
BuOH	1.41 ± 0.01	11.04 ± 0.05
EtOH	1.43 ± 0.01	10.71 ± 0.03
MeOH	1.41 ± 0.01	10.28 ± 0.04
CHCl_3	1.67 ± 0.02	9.13 ± 0.05
PBS	< 0.10	$\tau_1 = 0.08 \pm 0.01$ (W 72 %) $\tau_2 = 8.44 \pm 0.34$ (W 28 %)

Table 2. Fluorescence quantum efficiencies (QE) of compound **14a** and **14b** using ethanol, chloroform and PBS as solvents as solvent. Typically, the excitation was in the Soret band, 400–430 nm.

Solvent	QE (%) 14a	QE (%) 14b
EtOH	4.35 ± 0.03	13.2 ± 0.81
CHCl_3	4.22 ± 0.35	11.1 ± 0.81
PBS	0.097 ± 0.008	2.25 ± 0.003

Triplet excited state absorption (TESA) and singlet oxygen formation

As both the spectral and time-resolved features of the excitation/emission were essentially indistinguishable within the Zn- and proto-forms of the three glycosylated variants they were compared pairwise, proto- or Zn-form, in more advanced photophysical characterization of triplet states and singlet oxygen generation.

The compounds **14a** and **14b** were used to study the triplet excited state absorption (TESA). Here, samples dissolved in acetonitrile (typically 5–10 μM) were argon gas was used to purge out oxygen that strongly quenches the triplet signal. Upon laser excitation via one of the Q-bands (**14a**: 592 nm, **14b**: 517 nm) a white light flash pulse controlled by a pulse delay generator is used to probe the spectral transmission at a selected delay time (Figure 3). However, as the transient absorption spectrum is recorded, it also contains a large negative contribution from the depleted ground state (For details on how to process and interpret the TESA spectra, see

Glimstad et al.^[38]). Such spectra for the **14a** and **14b** at zero delay-time are shown in Figure 3A and 3B, respectively (black lines). In the plots are also showing the ground state absorption spectrum (red) and the resulting TESA spectrum (blue) formed by adding a fraction of the ground state absorption (red) to compensate the depletion.^[38] This results in the blue curves in Figure 3 as the 'true' TESA spectrum. It can be concluded from Figure 3 that the Zn- and proto-forms give very similar triplet absorption with the maxima shifted some 15–20 nm towards lower energy (red-shift) compared to the ground state absorption. Moreover, assuming that the transition dipole moment is similar for the Soret band in both the triplet and singlet state it can be estimated the fraction of formed triplet states are similar in both cases, in the range 36–41% of the total singlet absorption in the Soret band, used to compensate the depleted signal. By changing the delay, the TESA diminishes with time as expected. Fitting the apparent amplitude vs time one obtains the decay time of the triplet state raw data as shown in Figure S6, giving decay times of approximately 30 and 15 μs for the Zn- and proto-forms, respectively. These values are similar to triplet excited state life-times of related proto-form chlorins using toluene as solvent (approx. 50 μs), as reported by Pereira et al.^[26]

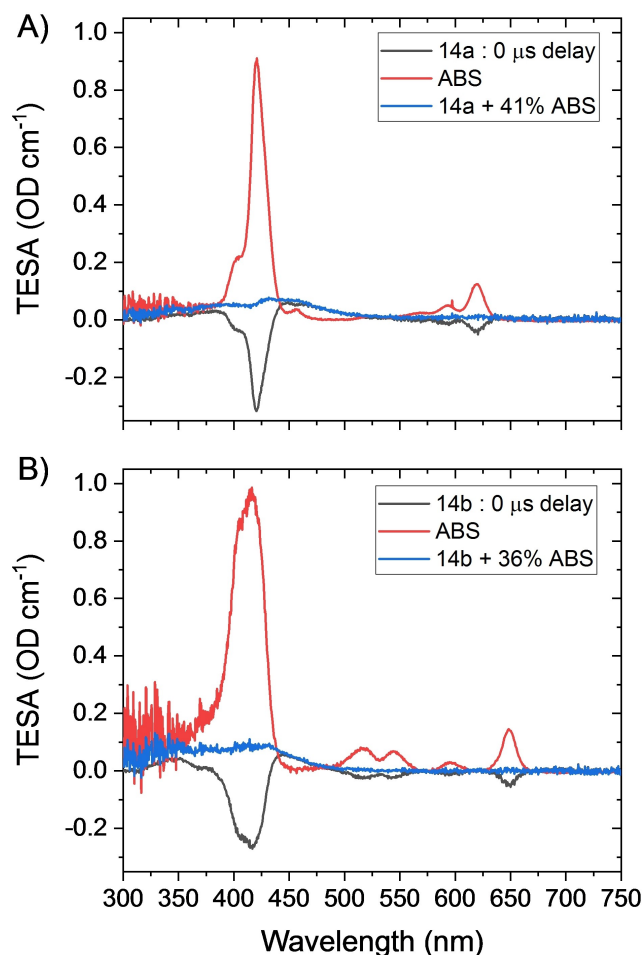


Figure 3. TESA spectra of a) **14a**: λ_{ex} = 592 nm, and b) **14b**: λ_{ex} = 517 nm in acetonitrile purged with argon. The black curve is the raw data showing the TESA in negative phase. The resulting blue curves are the corrected TESA by adding a fraction of the ground state absorption (red curves). See the main text for details.

Singlet oxygen luminescence – decay times and yield

In the type II PDT mechanism the triplet state of the excited photo-sensitizer collides with a ground state paramagnetic oxygen and an energy transfer mechanism occurs to form the toxic singlet oxygen utilized for biological action. The kinetics of the process is described by the following equations that we describe step-by-step.

Starting from the excited triplet of the photo-sensitizer [PS_T^*] (via absorption in the singlet ground state absorption and intersystem crossing) it decays according to the first order differential equation [Eq. (1)]:

$$\frac{d[PS_T^*]}{dt} = -k_{PS}[PS_T^*] - k_{TET}[O_2][PS_T^*] \quad (1)$$

Here, k_{PS} is the rate of decay in the solvent in absence of oxygen, corresponding to the triplet decay times discussed in the previous sub-section in oxygen-free solvents. The combined term $k_{TET}[O_2]$ is the rate of energy-transfers from the PS triplet to ground state oxygen O_2 , being dissolved in the same system in the vicinity of PS. Brackets means as usual concentration (unit: mol) and the units of the 1st order rates are 1/s whereas for the 2nd order triplet transfer rate k_{TET} it is 1/(mol · s).

The excited singlet oxygen O_2^* follows a similar differential equation, however, the energy-transfer term arises here as a source term with positive sign [Equation (2)]:

$$\frac{d[O_2^*]}{dt} = k_{TET}[O_2][PS_T^*] - k_{SO}[O_2^*] \quad (2)$$

The first term (2^{nd} order) is the product of ground state oxygen molecules and excited PS triplets forming excited singlet oxygen at rate k_{TET} per mol oxygen. The 2^{nd} term is the natural decay of the excited singlet oxygen diluted in the solvent with rate k_{SO} . Equation (1) is readily solved in terms of the time-evolution of the initiating excited PS-triplet giving Equation (3):

$$[PS^*]_T(t) = K \cdot e^{-(k_{\text{PS}} + k_{\text{TET}}[O_2]) \cdot t} \quad (3)$$

Here we have introduced the apparatus constant K (unit: mol) that reflects the initial number of excited PS, and thus light intensity, initial PS concentration, etc. Eq (3) is inserted into Eq. (2), to finally obtain the differential equation that governs the fate of the singlet oxygen excitation with the dissolved concentration of ground state oxygen molecules as one parameter [Eq. (4)]:

$$\frac{d[O_2^*]}{dt} = K \cdot k_{\text{TET}}[O_2]e^{-(k_{\text{PS}} + k_{\text{TET}}[O_2]) \cdot t} - k_{\text{SO}}[O_2^*] \quad (4)$$

The first term act as a source term and the rates combined in the exponential is the effects of the spontaneous PS triplet decay (without oxygen) and the quenching driven by the presence of dissolved ground state oxygen. The combined pre-factor describes the number of excited triplets and the efficiency of transfer of energy to the ground state oxygen per second. Eq. (4) is readily solved (e.g., by applying the unilateral Laplace transformation) giving the time-evolution of singlet oxygen [Eq. (5)]:

$$[O_2^*](t) = \frac{K \cdot k_{\text{TET}}[O_2]}{(k_{\text{PS}} + k_{\text{TET}}[O_2] - k_{\text{SO}})} (e^{-k_{\text{SO}} \cdot t} - e^{-(k_{\text{PS}} + k_{\text{TET}}[O_2]) \cdot t}) \quad (5)$$

A similar expression has been proposed by Ogilby's group.^[39] Thus, from the time-evolution of the singlet oxygen concentration, in terms of luminescence as given by eq (5), it is possible to uniquely determine k_{SO} and the combined rate $k_{\text{PS}} + k_{\text{TET}}[O_2]$. Knowing the rate k_{PS} from a separate experiment, such as direct phosphorescence of the PS triplet, or kinetic excited state absorption, both in absence of oxygen, the combined rate constants can be further decomposed. To illustrate the effect of the various rate constants we present a simulation of Equation (5) with parameters relevant to the studied chlorins herein (Figure 4). The long decay decreasing with time corresponds to a decay time of 88 μs . This is typical for singlet oxygen in acetonitrile (Figure 5) and it translates to a decay rate $k_{\text{SO}} = 11235 \text{ s}^{-1}$.

The color-coded curves are for different rates of the exponential factor $k_{\text{TET}}[O_2]$ in the range 10^4 to 10^6 s^{-1} shown as insets and corresponds to the decay of the PS triplet due to quenching by oxygen (energy transfer to oxygen). Clearly, increasing this rate means better efficiency and more singlet oxygen as judged from the increase in overall amplitude and integrated area under the curves. The natural decay rate k_{PS} : Without oxygen we chose to correspond to 30 and 15 μs , solid and dashed lines, respectively. These values were taken from

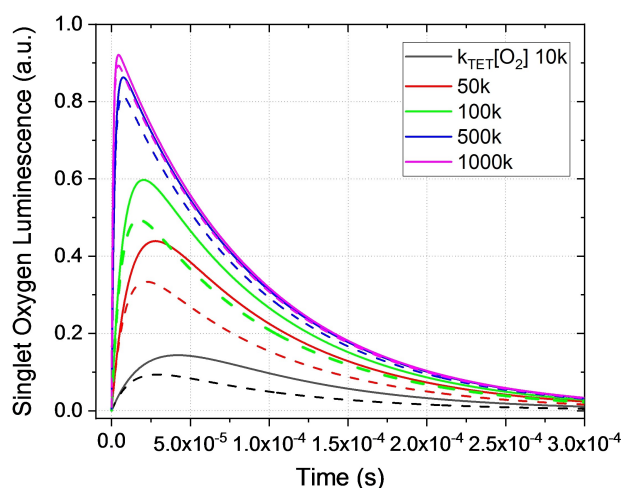


Figure 4. Simulation of singlet oxygen luminescence transients following Equation (5) and parameters described in detail in the text. The solid and dashed curves are for the situations with PS triplet decays of 30 and 15 μs , respectively, in the absence of oxygen in acetonitrile.

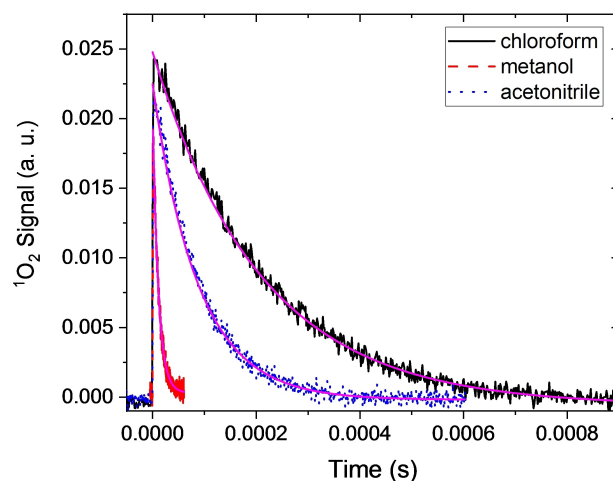


Figure 5. Transient singlet oxygen luminescence of **14a** around 1275 nm in different solvents as indicated by the inset. The laser excitation was at 592 nm. The purple lines are fits to the decay with parameters as discussed in the text.

the results of kinetic transient absorption using the same solvent (Figure 3, Figure S6). At higher rate of the energy transfer relative the natural decay of the PS triplet, the effect of the latter becomes negligible. Usually, it can be assumed that the quenching by oxygen is dominating to allow setting the rate $k_{\text{PS}} = 0$ in the analysis.

Next, we compare the simulations with experimental transient singlet oxygen decays of **14a** in 3 different solvents: chloroform, acetonitrile and methanol (Figure 5). Here we have also plotted the simulation to a single exponential fit to the long-decay tail, corresponding to the rate $k_{\text{SO}} = 1/\tau_{\text{SO}}$, the decay of singlet oxygen by the solvent. There is a dramatic change in the life-times: $10.9 \pm 0.07 \mu\text{s}$ (methanol) $87.6 \pm 0.5 \mu\text{s}$ (acetonitrile); $208 \pm 0.7 \mu\text{s}$ (chloroform) as previously reported and discussed by Bregnhøj et al.^[40] The transient

singlet oxygen emission also gives a qualitative indication on the singlet oxygen quantum yield as shown in Figure S7, comparing **16a** with **16b** and comparing **16b** with the widely used TPC2a chlorin based PS.^[41]

The singlet oxygen yield was determined by integrating the luminescence at 1270 nm in steady state excitation of the Soret band using CHCl₃ as solvent. Representative spectra of **15a** and **15b** using Phenanthrone^[42] as reference are shown in Figure 6, here giving a yield of 68%, similar to values reported by Laranjo et al using DMSO.^[27] It should be pointed out that measured singlet oxygen yields can vary considerably as the 2nd order kinetics involving the triplet excited state of the PS and the singlet oxygen, both are usually solvent dependent.^[42,43] Based on their promising photophysical properties the glycosylated chlorins were subject to further studies of photoinduced biological effects and localization in two cancer cell models, AY-27 and T24.

Illumination sources and absorption of photosensitizers

The PS compounds were examined for use in PDT using two light sources (red and blue) and two cell lines (AY-27 and T24). Since the absorption spectra of the various PS and as well as the lamp used for illumination have quite distinct spectral bands, we first investigated the details of the overlap of the light source with the absorption of the various PS compounds

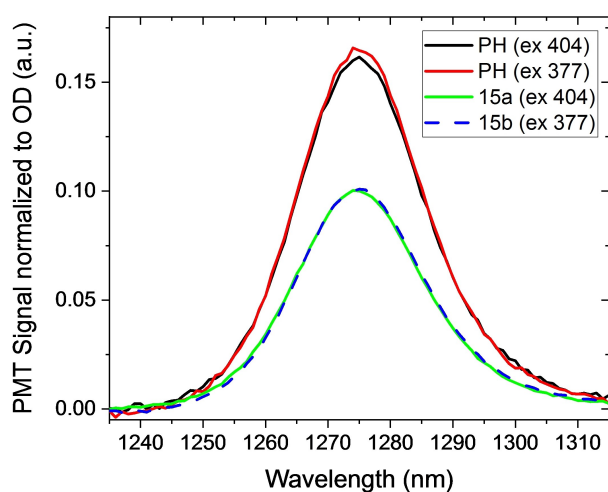


Figure 6. Singlet oxygen emission spectra used to estimate the singlet oxygen quantum yield (QY) for **15a** and **15b**. The singlet oxygen QYs for both **15a** and **15b** were calculated to 68% relative to the reference molecule phenanthrone (PH). The inset also indicate excitation wavelengths (404 and 377 nm).

Table 3. Results of the overlap for the different PS in PBS with the normalized illumination spectra. (For raw data, see Figure S8.) All values have been normalized to the overlap of **14a**.

Light source	6	14a	14b
Blue	1.67	1.90	1.43
Red	0.24	1.00	0.23

using PBS as solvent. As shown in Figure S8 the overlap between the lamp emission and the absorbance for each PS is different. The overlap was calculated by normalizing the lamp spectrum to its area, giving $(E(\lambda))$, and then integrate the overlap with the absorption i.e., the product $A(\lambda) \cdot E(\lambda)$, giving the results are summarized in Table 3. These numbers are then multiplied with lamp power and illumination time to obtain the relative dose. It should be mentioned that this is an approximate analysis based on the spectra obtained in PBS. For inorganic solvents (CHCl₃, THF) there is a distinct blueshift of the absorption bands, reducing the efficiency of **14a** in favor of **6** and **14b**. Nevertheless, this approach makes it possible to obtain a rough comparison of the relative PDT efficiency between different PS and light sources.

Viability assays

The transitional rat bladder AY-27 cell line is originating from a cell carcinoma whereas T24 (ATCC HTB-4) is a transitional cell carcinoma from human urinary bladder. The cells were incubated with the glycochlorin variants and **6** at different concentrations in complete cell culture medium for 24 hours. The incubated cells were thereafter illuminated by (blue light; 435 nm, 13 mW/cm²) or red light (633 nm, 29 mW/cm²) for varying amounts of time, typically 10–600 s. The survival of the cells was evaluated using the AlamarBlue assay post 24 hours. The cell survival relative untreated cells were then plotted vs. the relative dose, the latter calculated by multiplying the illumination time, spectral overlap (Table 3) and the lamp power.

The PDT effects of the unglycosylated chlorin **6** is compared with the glycosylated variants **14a** and **14b** at 5 μM concentration in AY-27 cells using blue light (Figure 7). Clearly, all

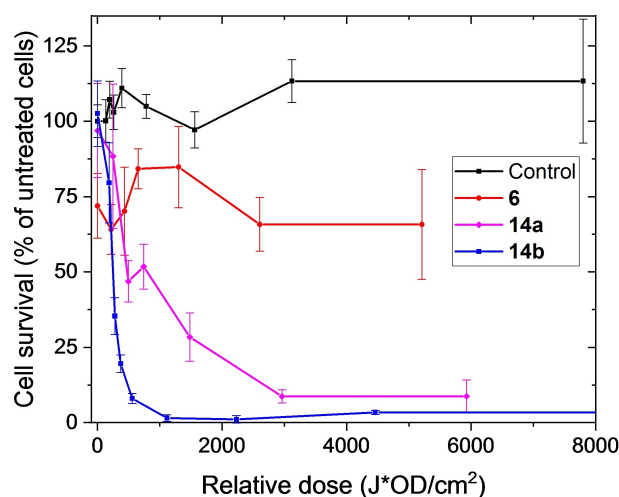


Figure 7. The cell survival (AlamarBlue assay) of AY-27 cells post PS and blue light treatment (435 nm) or light only. The PS were unglycosylated (**6**) and glycosylated (**14a** and **14b**) chlorin as shown in the inset, all at 5 μM. The relative dose was calculated using the overlap parameters in Table 3 multiplied with the illumination time (seconds) and lamp power (W/cm²). Control means light only.

three variants show photo-damaging although the rate is strongly dependent on the PS and increases in the order $6 < 14a < 14b$. The trend illustrates that glycosylation of the chlorin scaffold renders more effective PDT treatment. This is evident from the fact that the cell survival for glycol-compound **14b** went down to around zero at a relative dose of 2000 (corresponding to 60 s illumination), while it stayed above 60% for unglycosylated chlorin **6**.

Further cell survival analyses of compound **6**, **14a** and **14b** at various concentrations (0–50 μM) verified this trend (Figure S9A–C). This can be attributed to the increased water-solubility of the glycovariants as compared to **6**, and/or to an active transport into the cells via targeting glucose transporter (GLUT) receptors.^[44]

As **14b** showed the most promising result, all three proto variants (**14b**, **15b**, **16b**) were then compared together, showing very similar PDT efficiency for all three glycosylation moieties within experimental accuracy (Figure S9D). This is in agreement with the findings from results presented and discussed in previous sub-sections, i.e. the glycosylation moiety has very little effect on both the basic photo-physics and thus, the photo-activity.

Correcting for the spectral overlap of the illumination source and the PS it is possible to compare the effects of blue and red light illumination (Figure 8). Here we have also included results of the T24 cell model. As evident from the plots, the proto variant (**14b**) gives the most efficient PDT effect in all cases. The Zn-variant needs approximately 2–3 times higher effective doses to reach the same cell death fraction upon treatment.

The plots of the cell survival upon PS-only treatment (dark toxicity) are shown in Figure S10. The effect of **14a** and **14b** on both AY-27 and T24 cells shows small cell killing at 0.1–2 μM . At higher concentrations it increases gradually and above

10 μM the cell killing is substantial. As for other cell killing studies on the AY-27 line, both amphiphilic corroles^[45] and one Ruthenium porphyrin compound^[46] have shown a relatively fast cell killing (LD50 at about 8 min) with the same blue light source after incubation with low concentrations (10–20 μM) of the PS. For the T24 study on hexylaminolevulinic acid incubation, the protoporphyrin IX production results in effective cell death post both blue and red-light treatment.^[47]

Flow cytometry and PS cell localization

Flow cytometry is a powerful analysis method where information from single cells is recorded.^[48] In brief, a cell suspension is stained with fluorescent dyes to detect various key parameters e.g., apoptosis, cell division and other biomarkers.^[49] Scattered light is also recorded; the side scattered light (SS) reporting on complexity/granularity of the cells, whereas forward scattered light (FS) contain information of the size of the cell.^[50] In order to complement the results in Figure 7 and 8, flow cytometry was carried out on the AY-27 and T24 cell lines treated with **14b** (5 μM) and red light (633 nm). Samples were labelled with Alexa Fluor 488 annexin V and propidium iodide (PI) 24 hours after illumination according to the commercial protocol.^[51]

Annexin-V (here Alexa Fluor 488 annexin V) binds with phosphatidylserine on the outer plasma membrane leaflet, an indication of early and late apoptosis, whereas the PI response is indicating permeability of the plasma membrane as it intercalates with released DNA.^[48,49] Confocal images of the cells prepared for flow were taken and showed an uptake of the fluorophores in the expected manner (data not shown). Control experiments were carried out in an identical manner, but without the presence of PS.

The FS and SS results for the control cells were used to set a gate around the population ('E' in Figure 9). Further analyses were carried out on the gated cells, as the data points outside were assumed to be cell fragments, doublets and other anomalies. For AY-27 control cells, the FS and SS results show two distinct healthy populations within the gate E, the left population, which contains cells of a smaller size, could be cells in the G0-phase of cell cycle or the start of the G1-phase. The right population, which contains cells of larger size, could be cells in the G2-phase or the beginning of mitosis. AY-27 is more rapidly dividing than T24 cells (Figure S11), which could explain why two populations are seen in the AY-27 cells and not the T24. It was noted that **14b** shows slight fluorescence in the gate used to measure PI when excited by the 488 nm laser. This was considered when setting the horizontal gate. For the AY-27 cell line debris or cell fragments can be seen floating around in the suspension.

Representative results of AY-27 using the fluorescence channels are shown in Figure 10. Here the top panels are with the PS and after 0 s or 60 s of illumination (A,B). The lower panels are for the control experiment without PS (C,D). Upon annexin-V and PI treatment, the necrotic signal of AY-27 cells was roughly the same with and without **14b** incubation (11%–12%). After 60s of light, the PS treatment resulted in necrotic

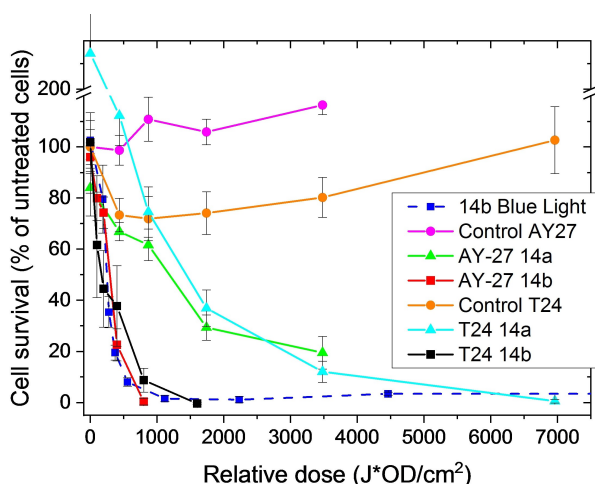


Figure 8. The cell survival (AlamarBlue assay) of AY-27 and T24 cancer cell lines treated with glycochlorin **14a** and **14b** (5 μM) under red light illumination. Control cells are only treated with red light. The error bars show the 95% confidence interval of the mean value. The result of **14b** with AY-27 using blue light from Figure 7 is plotted for comparison (blue squares; dashed curve is included to guide the eye).

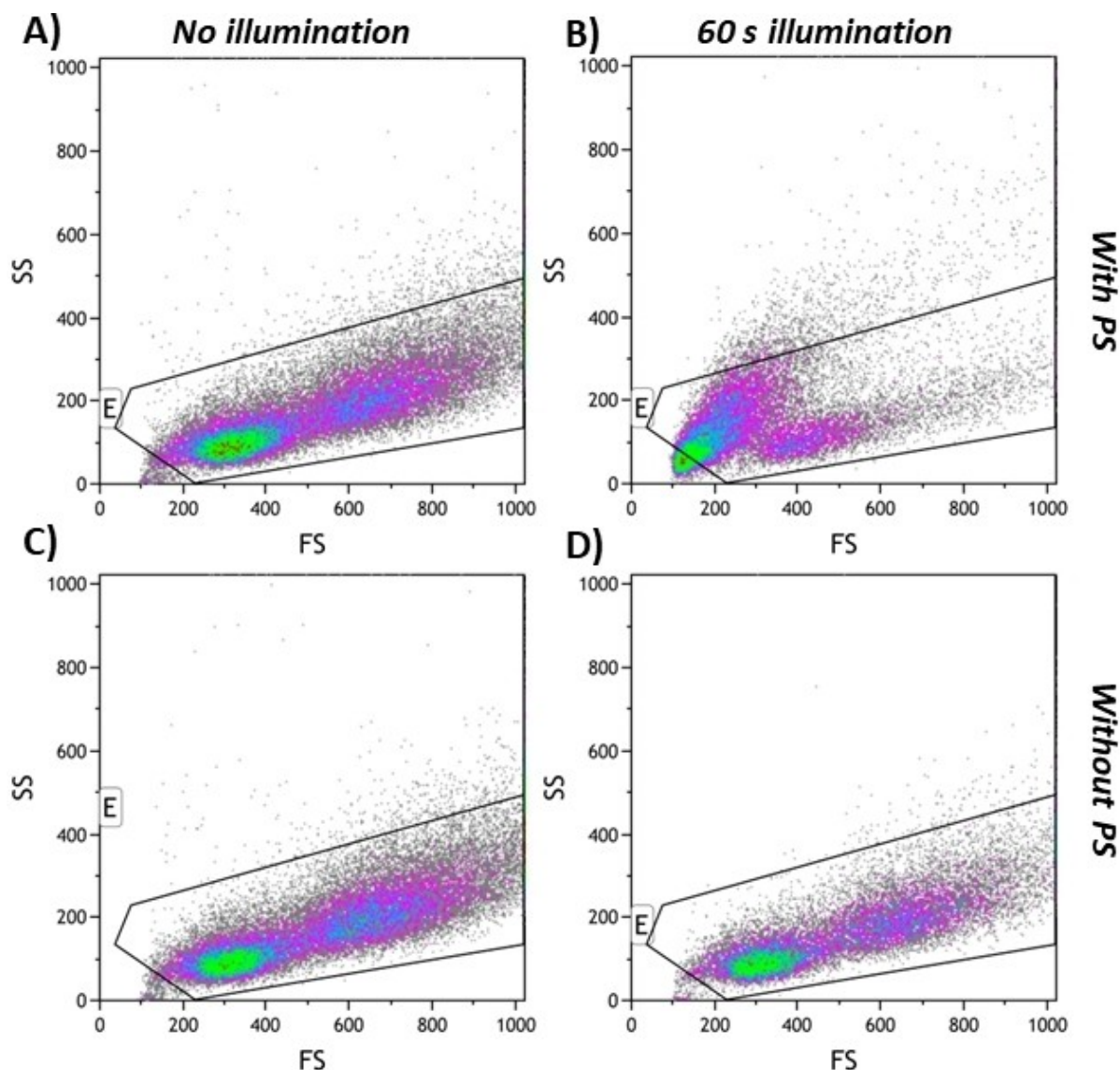


Figure 9. Side scatter and forward scatter plots of AY-27 and **14b** as described in the main text. (A,B) With **14b**. (C,D) Control experiment without **14b**.

cells (32%) and some increase in the apoptotic cell death (30%). The light effects on cells without PS was almost of no importance regard to apoptosis. Thus, there is a clear increase of both the PI and Annexin-V response for the illuminated sample with the PS. Taken together, this indicate that both necrotic and late apoptotic processes are active, following the PDT treatment with involvement of the immune system in addition to the classic apoptosis pathway. Furthermore, there is substantial counts in the lower right quadrant, indicative of also early apoptosis.^[49] Similar results were obtained using the T24 cells as shown in Figures S11 and S12.

In the non-illuminated AY-27 cells treated with **14b** the population of smaller cells contained more cells than in the control, this could be because more cells were arrested in the cell cycle and the cells were not dividing as rapidly. For the illuminated cells treated with **14b**, the population of smaller cells becomes more and more prominent until it is the only population present after 60s of illumination. The difference

between the amount of cells in the different quadrants of the control and the treated cells illuminated for 0 s or 30s was negligible (Figure S13), while the cells illuminated for 60s had a high percentage of dying cells (Figure 10). Therefore, most of the difference in viability seen in the AY-27 cells following 30s of illumination comes from the cells not dividing as rapidly as the population of larger cells was smaller, while after 60s cell death through apoptosis and necrosis influences the viability. The non-illuminated T24 cells, treated with **14b** were nearly identical to the control cells. This indicates that long term survival will also be similar and that the dark toxicity was low. The cells that have been exposed to light show more cells going through apoptosis and necrosis than for the control cells.

It should be pointed out that the forward scatter (FS) and side scatter (SS) results show how the amount of debris and therefore fragments of cells increase with longer illumination time. As mentioned earlier, including them in the results, it would skew the results as one cell will break into multiple

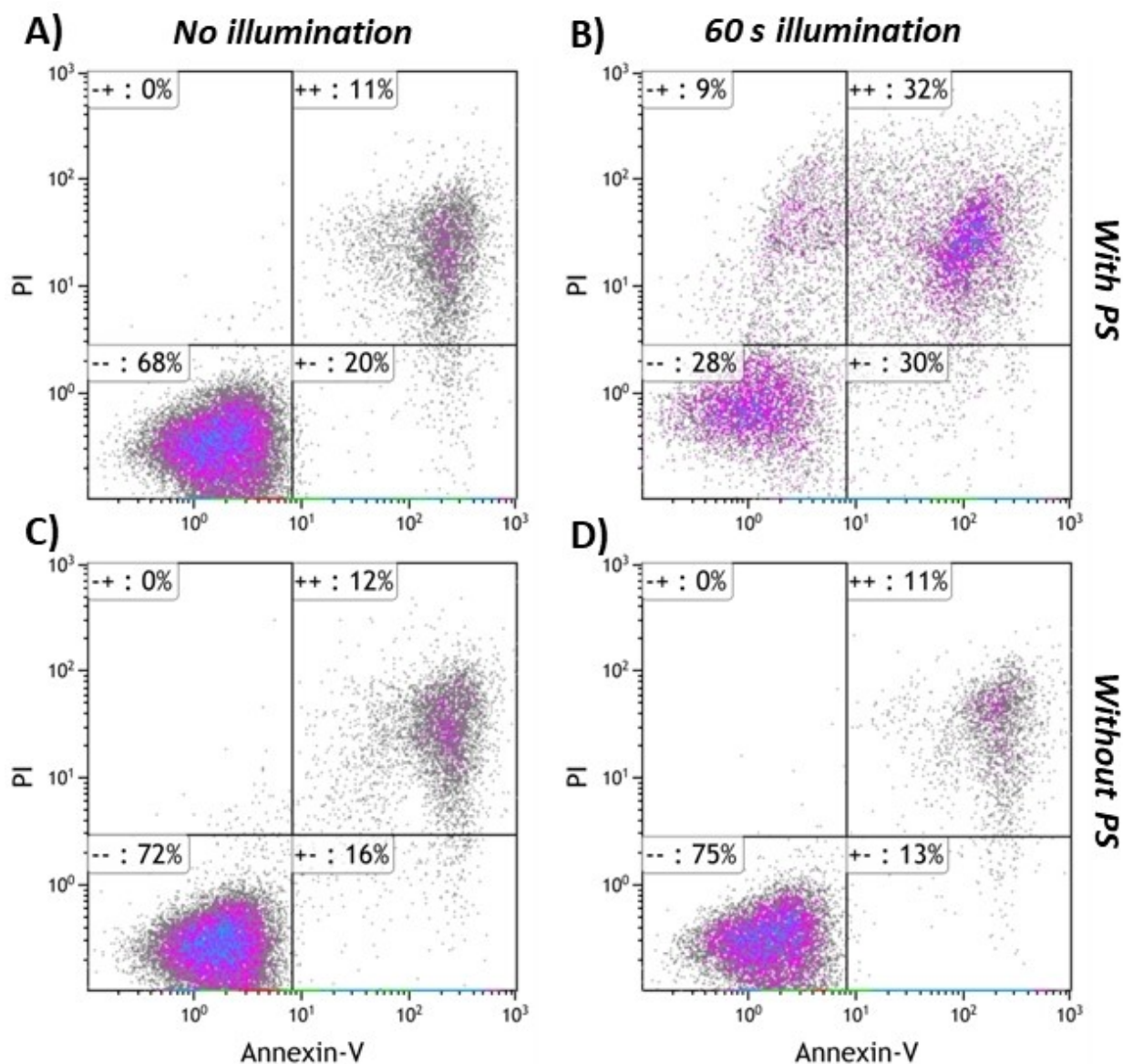


Figure 10. Signals from fluorescence channels for detection of annexin-V and PI in AY-27 cells treated with **14b** as described in the main text. (A,B) With **14b**. (C,D) Control experiment without **14b**.

fragments. But the presence of them indicates more cells than analyzed being dead. However, comparing the flow cytometer results for the control cells for both cell lines, it was evident that the cells without the presence of a PS were not affected by the illumination.

Selected cell experiments were imaged using differential interference contrast (DIC) and laser scanning confocal microscopy, the latter utilizing the fluorescence property of the PS to obtain information of its localization in the cells. Representative images of AY-27 cells are shown in Figure 11. The top row shows untreated cells without PS. The middle row illustrates the effects upon incubating the cells with the chlorin compound **14b** (pre-illumination). Upon PS incubation, the cells appear slightly rounded with well-defined clusters of PS fluorescence implying accumulation in some organelles. The bottom row shows AY-27 cells post 60s of light illumination,

which clearly indicate cells undergoing structural swelling decomposition. Similar results were obtained in the PS incubated T24 cell model (Figure S14).

To investigate the localization of the PSs in the cell, co-staining experiments were performed with different organelle markers comparing the unglycosylated **14b** in AY-27 cells. Staining across the cell layers was observed implying accumulation into high-signal clusters (Figure 12). Co-staining with LysoTracker Blue, a marker for lysosomes, demonstrated some co-occurrence. Further detailed colocalization studies were performed for **14b**, using stains for lysosomes, mitochondria and the cell membrane, where colocalization was evaluated at different incubation periods (2, 4, 8 and 24 hours) in AY-27 cells. The Maunders correlation coefficient^[52] was calculated for each time-point (Figure 13).

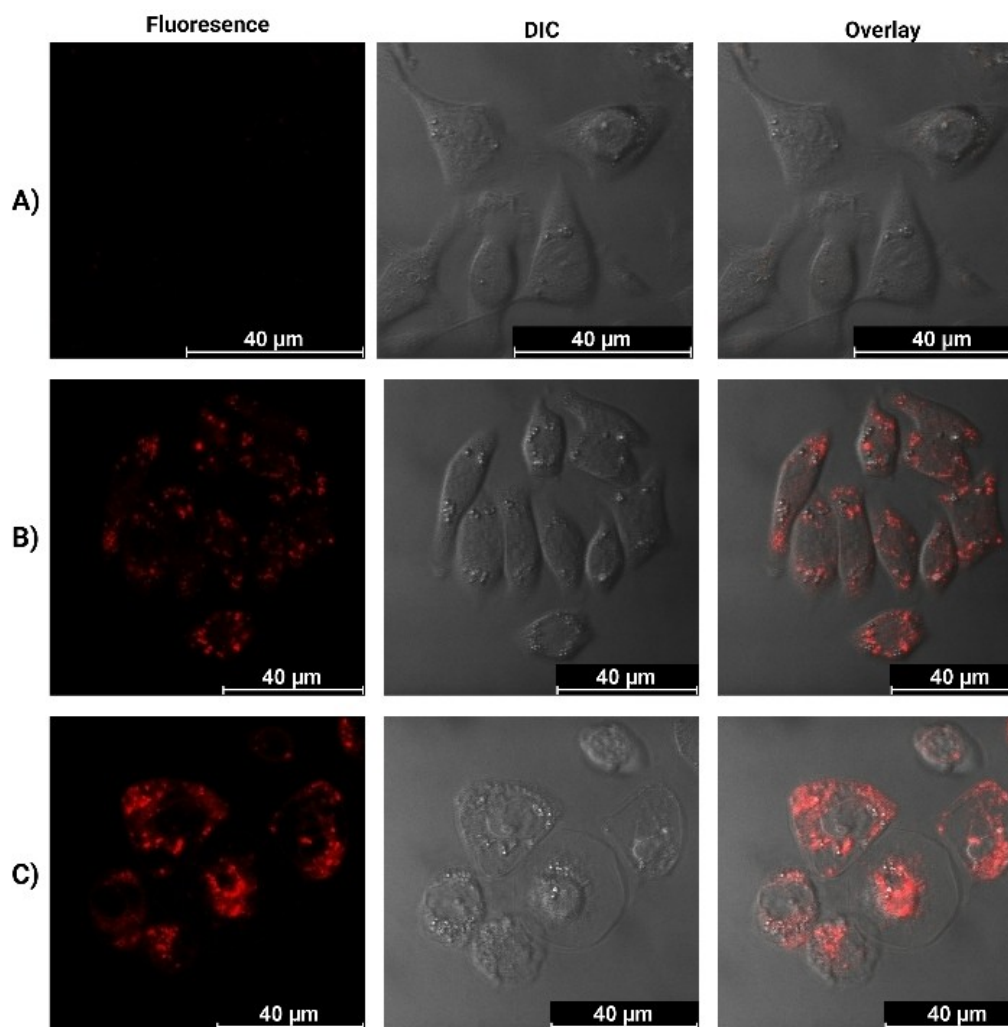


Figure 11. Confocal microscopy images of AY27 cancer cells. A) Control cells; B) incubated with **14b** (5 μ M, 24 h); C) incubated with **14b** (5 μ M, 24 h) and illuminated with red light ($\lambda = 633$ nm) for 60 seconds.

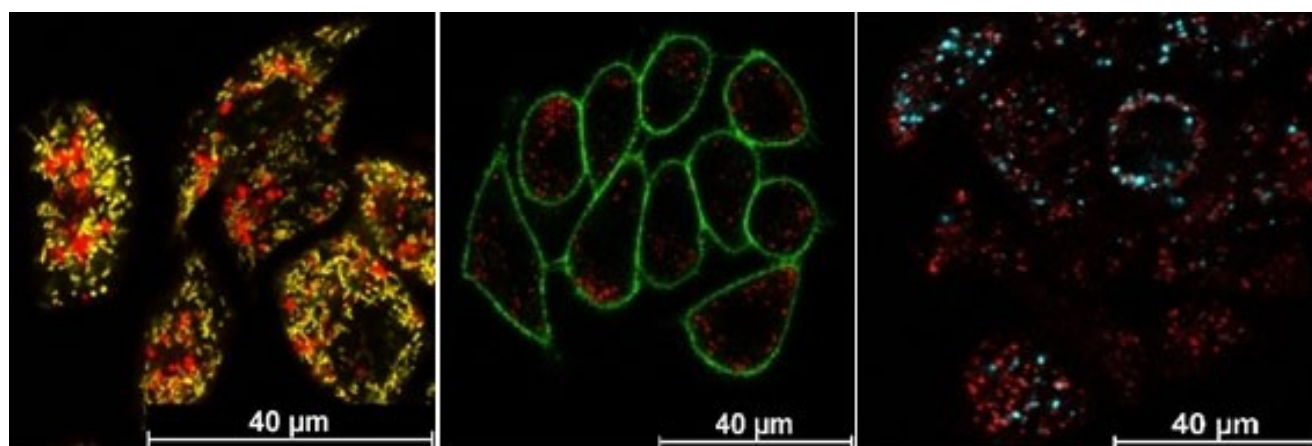


Figure 12. Representative images used for colocalization analysis. AY-27 cells incubated with CellMask Green (green), LysoTracker Blue (turquoise) or MitoTracker Orange (yellow) and **14b** (red). These were taken for cells incubated with PS for 4 hours.

Initially the colocalization of PS is similar between 0.2–0.25 for all three stains however, the M1 coefficient of LysoTracker

substantially increases with time to 0.5 after 24 hrs. For Mitotracker and Cell mask it remains essentially unchanged

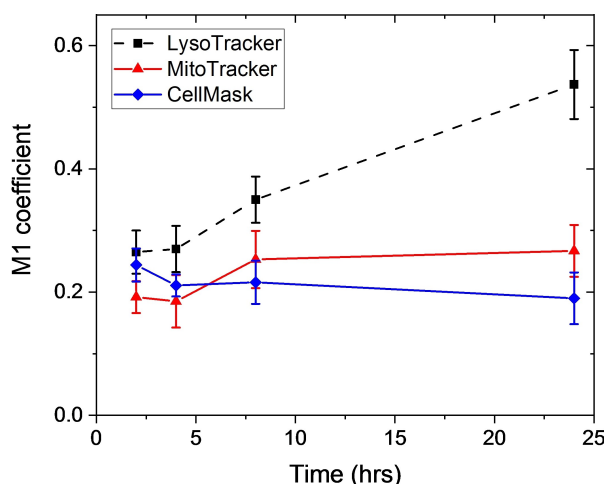


Figure 13. The M1 correlation coefficient of fluorescence from **14b** and cell markers LysoTracker Blue, MitoTracker Orange and CellMask Green, respectively, after various incubation periods of **14b** in the AY-27 cell line.

after a few hours of incubation. These results, together with the observation of clustered signal pre-illumination from Figure 12, suggest that approximately 50% of the PS accumulates in the lysosomes over time, which then rupture during PDT treatment, diffusing the PS in the cytosol.

Conclusions

We have successfully demonstrated a convenient synthetic approach to produce diglycosylated chlorins through the Cu(I)-catalyzed click conjugation reaction between the stable 4,5,6,7-tetrahydropyrazolo[1,5-a]pyridine fused chlorin scaffold and azide-functionalized carbohydrates. A set of three glycochlorins was synthesized featuring either glucose, galactose, or N-acetyl glucosamine on the proto-form macrocycle. The glycochlorins were characterized for the PDT-relevant photophysical properties, displaying significant absorption within the therapeutically applicable wavelength range and good singlet oxygen quantum yields. All three carbohydrates (glucose, galactose and N-acetyl glucosamine) were found to exert very similar photophysical properties. Results from comparative biological studies of the synthesized PSs in the AY-27 and T24 cancer cell models showed substantially increased photocytotoxic for the glycochlorins as compared to the unglycosylated chlorin. This might be based on an enhanced cellular uptake of the glycoconjugates. Among the glycochlorins, the proto-form was found to be 2–3 times more efficient than the Zn-stabilized variant for both red and blue light illumination, despite similar triplet and singlet oxygen yields. Provisional cell localization and flow cytometry studies of the proto-form showed that the PS localized mainly to lysosomes but also at other cell compartments, resulting in an mixed apoptotic and necrotic cell death mechanism, although the former dominated. Overall, we have succeeded to synthesize and to evaluate novel glycochlorins as improved PDT agents potential for cancer therapy.

Experimental Section

Experimental details including details on chemical synthesis and NMR spectra of the compounds are found in the supplementary information. Concerning their stability, no systematic studies were made but we observed that there was no noticeable degradation of samples after 2 years of -18°C storage (powder, DMSO stock solutions) or several weeks diluted in solvents, stored in the dark in a regular fridge ($+5^{\circ}\text{C}$).

Basic optical spectroscopy

The samples were received as 1.5–10 mM stock solutions in DMSO. Small amounts diluted down to typically 1–5 μM using 1 cm pathlength/3 ml quartz cuvettes for photophysical studies. Steady state absorption spectra were recorded using a Shimadzu UV-1601PC spectrophotometer. Measurements were performed with 10 mm quartz cuvettes (Hellma Precision) with a Teflon cap allowing for gas-purging using syringe needles. Steady state photoluminescence measurements were carried out employing a PTI Quantamaster 8075-22 (Horiba Scientific) equipped with Double Mono 300 spectrometer chambers for both excitation and emission. A Hamamatsu R928 PMT was used for detection in the range 185–950 nm. A OB-75X (75 W Xenon arc lamp) was used as the light source. For singlet oxygen luminescence a detection port of the spectrometer was directed to a 1427C-AH detector coupler together with a liquid nitrogen cold Indium-Gallium-Arsenide solid state detector (Horiba Scientific: DSS-IGA020). Data acquisition and basic data-handling of steady state luminescence data were carried out with the Felix Data Analysis software and further processed and presented using Origin Pro. Time-resolved fluorescence decays were recorded using an IBH time-correlated single photon counting (TCSPC) spectrometer system with 1 nm resolved emission monochromator (5000 M, Glaskow, UK). The system was equipped with a TBX-04D picosecond photon detection module and the sample was excited using an IBH LED operating at 469 nm. The measured decay-trace was analyzed using deconvolution fitting with the IBH Data Station v 2.1 software. For more details on the procedures, see Glimsdal *et al.*^[38]

Quantum efficiency (QE)

Coumarin 153^[53] and Zn-TPP^[54] were used as reference materials for the investigated molecules. The latter was measured to have a quantum yield of 0.028 ± 0.001 (ethanol) by comparison with sulphorhodamine 101 (QE: 0.95 ± 0.02).^[55] To reduce inner-filter and re-absorption effects, the absorbance values of the samples used were kept near or below 0.1. In all QY measurements. Measurements of integrated fluorescence were taken for typically 3–4 absorbance values, and their gradients were found through linear regression, see Rurak and Spieles,^[53] Glimsdal *et al.*^[39] for more details.

Lifetime measurements

Time-resolved fluorescence decays were recorded using an IBH time-correlated single photon counting (TCSPC) spectrometer system with 1 nm resolved emission monochromator (5000 M, Glaskow, UK). The system was equipped with a TBX-04D picosecond photon detection module and the sample was excited using an IBH LED operating at 469 nm. The measured decay-trace was analyzed using deconvolution fitting with the IBH Data Station v 2.1 software. For more details on the procedures, see Glimsdal *et al.*^[38] The chlorins were dissolved in THF and were excited at $\lambda = 403$ nm.

Laser flash photolysis measurements

The flash photolysis measurements were performed using a laser flash photolysis spectrophotometer from Applied Photophysics (LKS.80, Leatherhead United Kingdom) and a Nd:YAG Laser System (EKSPLA NT342B-SH-10-WW, Vilnius Lithuania). The differential absorption spectra with microsecond time resolution were acquired using an ungated 2048-channel spectrograph (BWTek model BRC642E) covering the 190–1100 nm spectral range. The sensor array is a back-thinned CCD, enclosed within the unit containing the dispersing device. The probe beam, traveling at a right angle to the laser beam, was derived from a compact xenon flash lamp (Hamamatsu L9456-01) that delivers an intense flash of about 1 μ s in duration (with FWHM of about 500 ns). The transmitted part of the probe beam was received by an optical fiber connected to the spectrograph. Let $S_k^{\pm\pm}$ denote the output of the k th channel, where the first (second) superscript indicates whether a shutter blocking the probe (pump) beam is open (+) or closed (–). Laser-induced changes in the absorbance of the sample at each channel were calculated using the following equation [Eq. (6)]:

$$\Delta A_k = \log[(S_k^{+-} - S_k^{--}) / (S_k^{++} - S_k^{--})] \quad (6)$$

Unless otherwise mentioned, the absorption spectra were measured at a 1 μ s delay between the pump (laser) and probe (flashlamp). The BWTek software allows for the detection of three spectra, so S^{+-} , S^{++} , and S^{--} were measured. The S^{--} spectrum (no probe, laser pulse) contains fluorescence from the sample, which is restricted to a limited wavelength range. The background noise of BWTek is wavelength-independent (the S^{--} spectrum; no probe, no laser) and is therefore taken to be the diode readings outside the fluorescence range. The spectra were imported to Excel where ΔA_k was calculated. The time resolution of this instrument is limited by the duration of the laser pulse (6 ns).

Transient Singlet Oxygen Luminescence Measurements

The singlet oxygen luminescence lifetime and yield were measured from the transient luminescence of a solution containing the dye in a standard 90° configuration. A tunable OPO laser, NT342A-SH-10-WW (Ekspla, Lithuania) was used for excitation. Typically, pulses of energy 15–20 μ J were used. For transient recording, a PMT (R5509, Hamamatsu) and a bandpass interference filter with maximum transmission at 1272.5 nm and a long pass filter transmitting above 780 nm) were used in conjunction to avoid spurious signals. An Infiniium BDSU Oscilloscope (Keysight, United States) was used to collect and monitor data. Time-gated electronics was used to control the time between the laser excitation and the recording of the luminescence transient. To obtain a reference signal (minimum amount of air/oxygen) the sample cell was bubbled with argon gas for 10 min.

Optical and fluorescence microscopy

The medium was removed and each well was washed (PBS×3) before incubation with the appropriate stains for the appropriate amount of time. The cells were imaged employing a confocal laser scanning microscope (Leica TCS SP8 MP, Leica Microsystems, Germany). The objective used was HC PL APO CS2 63×/1.40 OIL, with oil as immersion liquid with refractive index 1.518. The lasers used was a =405 nm laser and a tunable White Light Laser (WLL) with range from =470 nm–670 nm.

Cell cultivation

The AY-27 cell line originates from a transitional cell carcinoma in a rat bladder and was supplied by Professor Steven H. Selman from the Medical College of Ohio, Toledo, USA in 2004. The human T24 cells originate from a female's transitional cell carcinoma of the bladder and were supplied by the group of Prof. Barbara Krammer, University of Salzburg, Austria. The two cell lines were kept separate during the experiments and were not in the sterile cell bench at the same time to minimize chances of cross-contamination. The AY-27 cells were grown in RPMI-1640 Growth medium (Catalogue No. 21875091, Gibco), containing 10% fetal bovine serum (Catalogue No. F-7524, Sigma Aldrich), 1% penicillin/streptomycin (10 U/mL/10 g/mL, Catalogue No. P-0781, Sigma Aldrich) as well as 0.33% L-glutamine (200 mM, Catalogue No. G-7513, Sigma Aldrich). The T24 cells were grown in DMEM medium (Catalogue No. 11960044, Gibco) containing 10% fetal bovine serum, 1% penicillin/streptomycin, 0.33% L-glutamine and 1 mM of sodium pyruvate (Catalogue No. S8636, Sigma Aldrich). Both cell lines were grown in sterile 75 cm² culture flasks. The cells were kept in an incubator at 37 °C in a humidified atmosphere containing 5% CO₂. Twice a week, after reaching 80–90% confluence, the cell cultures were split. The medium was removed from the flask and the cells were washed once in phosphate-buffered saline (PBS) to discard dead cells and traces of old medium. The cells were detached from the flask by adding trypsin/ethylenediaminetetraacetic acid solution (3 mL, 0.25%/0.02%, Catalogue No. T-4049, Sigma Aldrich) and incubated (37 °C, 5 min). The trypsinated cells were then transferred to a test tube and centrifuged at 1500 RPM for 5 min. A cell suspension of known concentration was formulated. From this suspension, two new flasks (2 million cells, 0.5 million cells) were sown and medium added for a total of 15 mL per flask. In addition to the sub-culturing, the cells underwent medium change and washing in PBS once a week.

Photodynamic therapy

The cells were trypsinated, centrifuged, and counted as previously described. The cell suspension was further diluted to make a concentration of 0.015×10⁶ cells/mL. The cell suspension (200 μ L/well) was then added to 96-well black plates (Costar® Corning incorporated, Catalogue No. 3603, Sigma Aldrich) by multi-pipette. The cells were further incubated for 24 h for AY-27 or 48 h for T24 (37 °C, 5% CO₂). The next day, the medium in the dishes was removed, and cells were washed once with PBS. The PSs was then mixed with new growth medium in varying concentrations. The medium containing the PS was distributed some of the rows. The control rows and rows only receiving light were refilled with the same amount of normal growth medium. From this point on, all plates were maintained under dark conditions using aluminum foil when not undergoing illumination. The cells were incubated for 24 h. Prior to illumination, the medium was removed from the dishes and the cells washed twice with PBS to remove any extracellular traces of the photosensitizer. Then, a small amount of PBS was added to cover the cells during the illumination process. Immediately after the removal of the medium and the addition of PBS, the cells were placed on the LumiSource® lamp (435 nm, 13 mW/cm²) or the custom made red-light source (633 nm, 29 mW/cm²) for the specified time.^[48] When removed from the lamp, the plates were quickly covered to avoid any excess illumination. The PBS was removed from the dishes and the cells were resupplied with growth medium and incubated overnight (24 h) before the AlamarBlue viability assay.

Flow Cytometry

To determine if cells were healthy and to determine modes of cell death, flow cytometry was employed. Alexa Fluor™ 488 annexin V binds to phosphatidyl serine. Phosphatidyl serine is, in healthy cells, located intracellularly, but in apoptotic cells it translocated to the outer surface of the cell membrane staining them green.^[52] Propidium Iodide (PI) binds to DNA but cannot penetrate the membrane of live cells, but penetrates dead or necrotic cells thereby staining them red. Using Alexa Fluor 488 annexin V and PI apoptotic cells will show green fluorescence, dead or necrotic cells will show green and red fluorescence while live cells will not show fluorescence. A 6 cm petri dish was employed where 3 mL of cell suspension (0.16×10^6 cells/mL) was seeded out and incubated for 24 h (AY-27) or 48 h (T24) (37°C , 5% CO_2). The PS was diluted in growth medium (5 μM) and the old growth medium was exchanged, the dishes were covered with aluminium foil to limit light exposure and incubated (24 h, 37°C , 5% CO_2). The cells were washed twice with PBS (1.5 mL, 37°C) and were illuminated in PBS (1.5 mL, 37°C), for 0 s, 30s, 60s or 90s. The red-light source (633 nm) was turned on and stabilized for at least 15 minutes prior to illumination. After light treatment, PBS was removed, and growth medium (3 mL, 37°C) was added. The cells were then left to incubate for 24 h (37°C , 5% CO_2) to let the damage manifest. The cells were trypsinated (1 mL/dish, 37°C) and stored at 37°C until disconnected (3 to 5 minutes). They were then suspended in growth medium (3 mL/dish, 37°C) and counted, before centrifugation (1500 RPM, 5 minutes). The medium was removed, and the cells were washed in cold PBS and re-centrifuged (1500 RPM, 5 minutes). The cell pellets were suspended in a 1X annexin-binding buffer to a concentration of 1×10^6 cells/mL. 100 μL of each sample was added to an Eppendorf tube with Alexa Fluor 488 annexin V (5 μL) and PI working solution (1 μL , 100 $\mu\text{g}/\text{mL}$ in annexin 1X) and incubated at room temperature for 15 minutes. After the incubation period 1X annexin binding-buffer (400 μL) was added to each tube and immediately put on ice and analyzed in Gallios Flow Cytometer (Beckman Coulter) [48]. At the flow cytometer the fluorescence was measured at 525/20 nm (FL1) and 620/20 nm (FL3) using 488 nm laser as the excitation wavelength. The analysis was carried out in Kaluza Analysis 1.3 (Beckman Coulter).

Localization studies using confocal microscopy

The AY-27 cells were trypsinated, centrifuged, and counted as previously described. The cell suspension was further diluted to make a concentration of 0.05×10^6 cells/mL and added to 8-well plates (300 $\mu\text{L}/\text{well}$) (Catalogue No. 80826, Ibidi) the cells were incubated for 24 h (37°C , 5% CO_2). The cells were then washed once with PBS and PS was added and incubated for varying amounts of time. After incubation, cells were incubated again with either MitoTracker Orange CMTMRos (50 nM, 100 μL , 45 min, 37°C , 5% CO_2), LysoTracker Blue (100 nM, 100 μL , 2 h, 37°C , 5% CO_2) or CellMask Green (1X, 5 min, 37°C , 5% CO_2) and imaged using a confocal laser scanning microscope (Leica TCS SP8 MP, Leica Microsystems, Germany). All of the emissions were detected through a 1 Airy Unit pinhole. The laser power, detector gain, and offset were chosen to minimize auto-fluorescence in the control samples where no photosensitizer was added. For further processing, 1024 by 1024-pixel images with an 8bit dynamic range were recorded. The assessment of the colocalization in the aforementioned experiments was based on an algorithm developed in-house using the Python 3 programming language. Colocalization was quantified using Manders Correlation Coefficients (MCC),^[52] using Costes' statistical method for defining the threshold value for each image.^[56] For details, see Bergvöll.

Acknowledgements

This work was supported by the Swedish Research Council (Grants No. 2016-00748). We thank Linnea Dahle (Nykode Therapeutics, Oslo) for valuable discussions and Astrid Bjørkøy and Sylvie Lelu for assistance in the microscopy and cell labs.

Conflict of Interests

The authors declare no conflict of interest.

Data Availability Statement

The data that support the findings of this study are available in the supplementary material of this article.

Keywords: chlorins · cytotoxicity · photodynamic therapy · photophysics · photosensitizers · singlet oxygen

- [1] E. Zenkevich, E. Sagun, V. Knyukshto, A. Shulga, A. Mironov, O. Efremova, R. Bonnett, S. P. Pinda Songea, M. Kassem, *J. Photochem. Photobiol. B* **1996**, 33, 171–180.
- [2] J. C. Kennedy, R. H. Pottier, D. C. Pross, *J. Photochem. Photobiol. B* **1990**, 6, 143–148.
- [3] P. Chinna Ayya Swamy, G. Sivaraman, R. N. Priyanka, S. O. Raja, K. Ponnuvel, J. Shanmugpriya, A. Gulyani, *Coord. Chem. Rev.* **2020**, 411, 213233.
- [4] J. Moan, K. Berg, *Photochem. Photobiol.* **1991**, 53, 549–553.
- [5] A. P. Castano, T. N. Demidova, M. R. Hamblin, *Photodiagn. Photodyn. Ther.* **2004**, 1, 279–293.
- [6] J. Min Park, J. H. Lee, W. D. Jang, *Coord. Chem. Rev.* **2020**, 407, 213157.
- [7] L. B. Josefsen, R. W. Boyle, *Theranostics* **2012**, 2, 916–966.
- [8] J. Hynek, J. Zelenka, J. Rathousky, P. Kubat, T. Ruml, J. Demel, K. Lang, *ACS Appl. Mater. Interfaces* **2018**, 10, 8527–8535.
- [9] P. Dharmaratne, D. N. Sapugahawatte, B. Wang, C. L. Chan, K.-M. Lau, K. P. Fung, D. Kp Ng, M. Ip, *Eur. J. Med. Chem.* **2020**, 200, 112341.
- [10] U. Chilakamarthi, L. Giribabu, *Chem. Rec.* **2017**, 17, 775–802.
- [11] S. Kwiatkowski, B. Knap, D. Przysupski, J. Saczko, E. Kedzierska, K. Knap-Czop, J. Kotlinska, O. Michel, K. Kotwski, J. Kulbacka, *Pharmacotherapy* **2018**, 106, 1098–1107.
- [12] K. Arja, M. Elgland, H. Appelqvist, P. Konradsson, M. Lindgren, K. P. R. Nilsson, *ChemistryOpen* **2018**, 7, 488.
- [13] H. Abrahamse, M. R. Hamblin, *Biochem. J.* **2017**, 473, 347–364.
- [14] A. C. Kübler, J. de Carpentier, C. Hopper, A. G. Leonard, G. Putnam, *Int. J. Oral Maxillofac. Surg.* **2001**, 30, 504–509.
- [15] E. V. Kochneva, E. V. Filonenko, E. G. Vakulovskaya, E. G. Scherbakova, O. V. Seliverstov, N. A. Markichev, A. V. Reshetnikov, *Photodiagn. Photodyn. Ther.* **2010**, 7, 258–267.
- [16] R. Baskaran, J. Lee, S.-G. Yang, *Biomaterials* **2018**, 22, 25, <https://doi.org/10.1186/s40824-018-0140-z>.
- [17] J. Laakso, G. A. Rosser, C. Szijjártó, A. Beeby, K. E. Borbas, *Inorg. Chem.* **2012**, 51, 10366–10374.
- [18] M. Kraye, E. Yang, J. R. Diers, D. F. Bocian, D. Holten, J. S. Lindsey, *New J. Chem.* **2011**, 35, 587–601.
- [19] N. V. S. Junior Gonzales, D. K. Bhupathiraju, D. Hart, M. Yuen, M. P. Sifuentes, B. Samarxhiu, M. Maranan, N. Berisha, J. Batteas, C. M. Drain, *J. Org. Chem.* **2018**, 83, 6307–6314.
- [20] M. Gałézowski, D. T. Gryko, *J. Org. Chem.* **2006**, 71, 5942–5950.
- [21] J. A. S. Cavaleiro, M. G. P. M. S. Neves, A. C. Tomé, *Arkivoc* **2003**, 14, 107–130.
- [22] M. M. Pereira, C. J. P. Monteiro, A. V. C. Simoes, S. M. A. Pintos, A. R. Abreu, G. F. F. Sa, E. Silva, L. B. Rocha, J. M. Dabrowski, S. J. Formosinho, S. Simoes, L. G. Arnaut, *Tetrahedron* **2010**, 66, 9545–9551.
- [23] N. A. M. Pereira, A. C. Serra, T. M. V. D. Pinho e Melo, *Eur. J. Org. Chem.* **2010**, 34, 6539–6543.

- [24] N. A. M. Pereira, S. M. Fonseca, A. C. Serra, T. M. V. D. Pinho e Melo, H. D. Burrows, *Eur. J. Org. Chem.* **2011**, 20–21, 3970–79.
- [25] N. A. M. Pereira, M. Laranjo, M. Pineiro, A. C. Serra, K. Santos, R. Teixo, A. M. Abrantes, A. C. Gonçalves, A. B. S. Ribeiro, J. Casalta-Lopes, M. F. Botelho, T. M. V. D. Pinho e Melo, *Eur. J. Med. Chem.* **2015**, 103, 374–380.
- [26] N. A. M. Pereira, M. Laranjo, J. Pina, A. S. R. Oliveira, J. D. Ferreira, C. Sánchez-Sánchez, J. Casalta-Lopes, A. C. Gonçalves, A. B. Sarmento-Ribeiro, M. Piñeiro, J. S. Seixas de Melo, M. F. Botelho, T. M. V. D. Pinho e Melo, *Eur. J. Med. Chem.* **2018**, 146, 395–408.
- [27] M. Laranjo, N. A. M. Pareira, A. S. R. Oliveira, M. C. Aguiar, G. Brites, B. F. O. Nascimento, B. Serambeque, B. D. P. Costa, J. Pina, J. S. Seixas de Melo, M. Pineiro, M. F. Botelho, T. M. V. D. Pinho e Melo, *Front. Chem.* **2022**, 10, 873245.
- [28] R. R. Allison, C. H. Sibata, *Photodiagn. Photodyn. Ther.* **2010**, 7, 61–75.
- [29] S. Desgranges, P. Juzenas, V. Vasovic, O. A. Glederaas, M. Lindgren, T. Warloe, Q. Peng, C. Contino-Pépin, *Biomedicine* **2022**, 10, 423.
- [30] R. J. Solá, K. Griebenow, *BioDrugs* **2010**, 24, 9–21.
- [31] S. V. Moradi, W. M. Hussein, P. Varamini, P. Simerska, I. Toth, *Chem. Sci.* **2016**, 7, 2492–2500.
- [32] S. Hirohara, Y. Kawasaki, R. Funasako, N. Yasui, M. Totani, H. Altimo, J. Yuasa, T. Kawai, C. Oka, M. Kawaichi, M. Obata, M. Tanihara, *Bioconjugate Chem.* **2012**, 23, 1881–1890.
- [33] M. Tamura, H. Matsui, S. Hirohara, K. Kakuchi, M. Tanihara, N. Takahashi, K. Nakai, Y. Kanai, H. Watabe, J. Hatazawa, *Bioorg. Med. Chem.* **2014**, 22, 2563–2570.
- [34] V. V. Rostovtsev, L. G. Green, V. V. Fokin, K. B. Sharpless, *Angew. Chem. Int. Ed.* **2002**, 41, 2596–2599.
- [35] C. W. Tornøe, C. Christensen, M. Meldal, *J. Org. Chem.* **2002**, 67, 3057–3064.
- [36] N. A. M. Pereira, M. Laranjo, J. Casalta-Lopes, A. C. Serra, M. Pineiro, J. Pina, J. S. Seixas de Melo, M. O. Senge, M. F. Botelho, L. Martelo, H. D. Burrows, T. M. V. D. Pinho e Melo, *ACS Med. Chem. Lett.* **2017**, 8, 310–315.
- [37] O. B. Sutcliffe, R. C. Storr, T. L. Gilchrist, P. Rafferty, *Tetrahedron* **2000**, 56, 10011–10021.
- [38] E. Glimsdal, M. Carlsson, T. Kindahl, M. Lindgren, C. Lopes, B. Eliasson, *J. Phys. Chem. A* **2010**, 114, 3431–3442.
- [39] M. K. Kuimova, G. Yahiolglu, P. R. Ogilby, *J. Am. Chem. Soc.* **2009**, 131, 332–340.
- [40] M. Bregnhøj, M. Westberg, F. Jensen, P. R. Ogilby, *Phys. Chem. Chem. Phys.* **2016**, 18, 22946–22961.
- [41] O. A. Glederaas A Johnsson, K. Berg, R. Manandha, D. Shrestha, D. Skåre, I. K. Ekroll, A. Høgset, A. Hjelde, *Photochem. Photobiol. Sci.* **2017**, 16, 1664–1676.
- [42] J. Godard, F. Brégrier, P. Arnoux, B. Myrzakhmetov, Y. Campavie, C. Frochot, V. Sol, *ACS Omega* **2020**, 5, 28264–28272.
- [43] F. Nifiatis, J. C. Athas, K. D. D. Gunaratne, Y. Gurung, K. M. Monette, P. J. Shivokevich, *The Open Spectroscopy Journal* **2011**, 5, 1–12, DOI: 10.2174/1874383801105010001.
- [44] V. Ganapathy, M. Thangaraju, P. D. Prasad, *Pharmacol. Ther.* **2009**, 121, 29–40.
- [45] R. F. Einrem, A. B. Alemayehu, S. M. Borisov, A. Ghosh, O. S. Glederaas, *ACS Omega* **2020**, 5, 10594–10601.
- [46] V. Bogoeva, M. Siksjo, K. G. Sæterbø, T. B. Melø, A. Bjørkøy, M. Lindgren, O. A. Glederaas, *Photodiagn. Photodyn. Ther.* **2016**, 14, 9–17.
- [47] L. Helander, H. E. Krokan, A. Johnsson, O. A. Glederaas, K. Plaetzer, *J. Biomed. Opt.* **2016**, 19, 088002.
- [48] K. M. McKinnon, *Current protocols in immunology* **2018**, 120, 259–269.
- [49] Z. Darzynkiewicz, E. Bedner, P. Smolewski, *Semin. Hematol.* **2001**, 38, 179–193.
- [50] L. de Rond, F. A. W. Coumans, R. Nieuwland, T. G. van Leeuwen, E. van der Pol, *Current protocols in cytometry* **2018**, 86, e43.
- [51] ThermoFisher Scientific: <http://www.thermofisher.com/no/en/home/references/protocols/cell-and-tissue-analysis/flow-cytometry-protocol/apoptosis/alexa-fluor-488-annexin-v-dead-cell-apoptosis-kit.html#prot2>.
- [52] E. M. M. Manders, F. J. Verbeek, J. A. Aten, *J. Microsc.* **1993**, 169, 375–382.
- [53] K. Rurak, M. Spieles, *Anal. Chem.* **2011**, 83, 1232–1242.
- [54] A. M. Brouwer, *Pure Appl. Chem.* **2011**, 83, 2213–2228.
- [55] S. V. Costes, D. Daelemans, E. H. Cho, Z. Dobbin, G. Pavlakakis, S. Lockett, *Biophys. J.* **2004**, 86, 3993–4003.
- [56] J. K. Bergvoll, “Localization of Novel Chlorin Photosensitizers and Commercial Stains in the AY-27 Cell Model Using Advanced Fluorescence Microscopy. 2021 Master Thesis, NTNU Norway,” <https://ntnuopen.ntnu.no/ntnu-xmlui/handle/2785587>.

Manuscript received: February 16, 2023
Revised manuscript received: May 21, 2023
Accepted manuscript online: May 22, 2023
Version of record online: June 26, 2023